Pure Appl. Geophys. 175 (2018), 2023–2044

https://doi.org/10.1007/s00024-018-1780-6

Pure and Applied Geophysics

Incidence Angles Maximizing the Goos–Hänchen Shift in Seismic Data Analysis

Stefano De Leo[1] and Rita K. Kraus[2]

Abstract—In the solid/liquid and liquid/solid scenarios, for the cases in which the P and S reflected waves are represented by complex amplitudes, we give the closed formulas for the Goos–Hänchen phase from which we can then determine the lateral displacements. We compare the results of the analysis done using the Zoeppritz equations with the calculations which appear in optics. We also discuss under which circumstances the plane wave analysis is valid and what happens for critical incidence, where divergences appear. For the liquid/solid interface, the incidence angles maximizing the lateral displacement are given as solutions of a polynomial equation.

Key words: Goos–Hänchen, Zoeppritz, interference.

1. Introduction

Seismic reflection is a method of exploring the Earth's crust by artificially generated waves (Upadhyay 2004; Ikelle and Amundsen 2005; Ashcroft 2011). When the wave vibrations meet the resistance of a different medium, they are reflected back as an echo. Geophysicists have mastered the technique of sound waves reflection and, using the fact that seismic amplitudes at each interface contain the physical properties just above and just below the boundary, employed reflection and transmission amplitudes in hydrocarbon detection, lithology identification, and fluid analysis. Seismic analysis essentially generates an ultrasonic image of the Earth. Special ships, fitted with equipment that produces seismic waves, are used to locate oil and gas. These waves fan out below the surface of the water, penetrating the seabed below and depending on what they hit (rock, oil, or gas) are reflected at different speeds back up towards the ship. There, seismometers record the waves and how fast they are travelling. These microphones are evenly spaced along a cable up to dozens of kilometers long, which is dragged behind the ship along the surface of the water. On land, vibrations are generated by vibrators, mounted on purpose-built vehicles. The data recorded by the seismometers is logged by powerful mobile computers. Using this method, it is then possible to explore as deep as dozens of kilometers with remarkable accuracy. Geophysicists process and analyze the collected data, with the help of computers, to generate detailed 3D models of the subsurface.

In geophysical exploration, we rarely deal with a simple isolated interface. However, our understanding of the variation of reflection and transmission coefficients with the incidence angle just begins with a single interface model. In this paper, we present a detailed analytical study of the Zoeppritz–Goos–Hänchen (ZGH) shift for P waves in liquid/solid interfaces and for P/S waves in solid/liquid interfaces. The Maxwell–Goos–Hänchen (MGH) shift is an optical phenomenon in which a light beam, when totally reflected from an interface between two dielectric media having different refraction indices, undergoes a lateral shift from the position predicted by geometrical optics. The lateral shift, conjectured by Isaac Newton in the 18th century, was experimentally observed, for the first time, by Goos and Hänchen (1947) and, 1 year later, theoretically explained by Artmann (1948) using the stationary phase method. Due to the smallness of the shift, the MGH lateral displacement can be macroscopically observed only by amplifying it by multiple reflections, as, for example, done in its first experimental detection, or using the technique based on the optical analog of the weak measurement in Quantum

[1] Department of Applied Mathematics, State of University of Campinas, Campinas, Brazil. E-mail: deleo@ime.unicamp.br
[2] Institute of Geoscience, State University of Campinas, Campinas, Brazil.

Mechanics (Aharonov et al. 1988; Duck and Stevenson 1989; Jayaswal et al. 2013), in which a combination of transverse electric and magnetic waves generates an outgoing optical beam characterized by two peaks, whose distance contains the information of the MGH shift.

Certainly, plane waves with their infinite wavefront do not represent physical beams as those used by geophysicists to collect data. Thus, calculations done using plane waves are surely useful to understand the problem, but have to be checked by a wave packet analysis. Nevertheless, the plane wave results often give the right behavior of physical beams. For example, most of the analytical expressions obtained, in optics, for the lateral displacement are based on a plane wave analysis. However, it is important to observe that the plane wave approach is valid for incidence angle out of the critical region:

$$\left[\arcsin\left(\frac{n_2}{n_1}\right)-\frac{\lambda}{w_0},\ \arcsin\left(\frac{n_2}{n_1}\right)+\frac{\lambda}{w_0}\right],$$

where λ is the wavelength of the optical beam, w_0 is its minimal waist, and $n_{1,2}$ is the refractive indices of the dielectrics above and below the boundary with $n_2 < n_1$. In the critical region, a wave packet analysis is, indeed, needed to remove the divergence found for incidence at the critical angle. In recent works Araújo et al. (2014a, b); Aráujo et al. (2016, 2017), closed-form expressions have been given in the critical region, where, due to the breaking of symmetry of the wave number distribution, an axial dependence is also present (Araújo et al. 2015; Santana et al. 2016).

The considerable number of publications on this subject demonstrate an increasing interest, not only in the optics community (Aiello 2012; Bliokh and Aiello 2013) but also in other fields such as particle physics (Bliokh and Aiello 2013), condensed matter (Ignatovich 2004), and geophysics (Ostrander 1984; Lerche 1990; Liu et al. 2008, 2012; Wang 2015). In this paper, we shall concentrate our attention on the lateral shift of P/S waves reflected by a solid/liquid interface and of P waves reflected by a liquid/solid interface, because in these scenarios, it is possible to obtain, using the matrix form of the Zoeppritz equations, closed forms for the reflection and transmission coefficients and consequently give analytical expressions for the Goos–Hänchen phase. This allows to compare the Zoeppritz critical regions and the lateral displacements with the ones given in optics and determine when additional critical regions appear and for which incidence angles maximal lateral displacements can be detected.

The main objective of this article is to provide seismologists with some of the fundamental mathematical background for understanding the role that Goos–Hänchen phase plays in the sound wave propagation. With the increasing power and continuous evolution of computers, numerical calculations and data analysis can be used for improving the resolution and accuracy of seismic images. However, analytical formulas are fundamental for understanding the propagation properties of sound waves. In this spirit, closed-form expressions for the ZGH phase allow to obtain polynomial equations from which the incidence angles maximizing the lateral displacement can be calculated. Starting from the results obtained in this paper, the authors hope is that new investigations, developments of the solutions, and possible applications could be stimulated in the Geophysics community.

The article is structured as follows. In Sect. 2, we fix our notation and, to leave the presentation self-contained, give, for an incident wave composed of a mixture of P and S waves, the unified matrix form of the Zoeppritz equations as well the energy flux partitioning at the interface. In Sects. 3 and 4, we respectively discuss the solid/liquid scenario for S and P waves, obtaining the analytical expressions for the reflection/transmission coefficients as well for the Goos–Hänchen phase. Then, in Sect. 5, we study the liquid/solid scenario for an incident P wave. Sect. 6 contains the analysis of the lateral displacements and, for the liquid/solid case, the polynomial equation from which the incidence angles maximizing the ZGH shift can be determined. In this Section, we also compare the seismic with the optical results and discuss the regions of the incidence angles for which the results obtained using the plane wave approach are valid. For the graphical presentation of our results, the liquid chosen was water and the solids: vegetal soil, wet sand and granite. Conclusions, remarks and outlooks are given in the final Section.

2. *The Matrix form of the Zoeppritz Equations*

To calculate the reflection and transmission coefficients, we assume that the seismic P and S waves can be treated as plane waves. Discontinuity between the first and second elastic medium results in compressive as well as shearing stress. Then, arriving at the interface that separates the two elastic media, both P and S waves are reflected back and transmitted away from the interface.

Two classical methods for obtaining the plane waves reflection and transmission coefficients are often quoted in seismology textbooks. In 1899, Knott gave the reflections and transmission coefficients by introducing unknown potential amplitudes into the continuity conditions. In 1919, Zoeppritz found a very similar set of reflection and transmission coefficients by letting the unknown potential amplitudes be displacement amplitudes. In this paper, we shall follow the notation and the matrix approach, based on the Zoeppritz method, given in the excellent book of Ikelle and Amundsen (2005) where the displacement amplitudes are replaced by the P and S wave potential amplitudes, scaled by their respective velocities. In this formalism, the case of an incident P wave can be treated simultaneously with that of an incident S wave. Choosing yz (z being the axis perpendicular to the interface separating the medium 1 from the medium 2, see Fig. 1) as the plane of incidence, an incident sound wave, containing a mixture (α, β) of P (represented by the potential amplitude Ψ) and S (represented by Φ) waves and moving in medium 1, will be represented by

$$\alpha\ \Psi_{\text{INC}} + \beta\ \Phi_{\text{INC}}, \tag{1}$$

with

$$\begin{aligned}\Psi_{\text{INC}} &= v_1\ \exp[\,i\,\omega\,(\,y\,\sin\psi_1 + z\,\cos\psi_1 - v_1\,t\,)\,/\,v_1\,]\\ \Phi_{\text{INC}} &= u_1\ \exp[\,i\,\omega\,(y\,\sin\varphi_1 + z\,\cos\varphi_1 - u_1\,t\,)\,/\,u_1\,],\end{aligned} \tag{2}$$

where $(v_1\,,\,\psi_1)$ and $(u_1\,,\,\varphi_1)$ are respectively the velocity and incidence angle of the P and S wave. Reaching the interface, the incident wave will generate reflected waves:

$$\begin{aligned}\Psi_{\text{REF}} &= v_1\,(\alpha\,R_{\text{PP}} + \beta\,R_{\text{SP}})\\ &\quad \exp[\,i\,\omega\,(\,y\,\sin\psi_1 - z\,\cos\psi_1 - v_1\,t\,)\,/\,v_1\,]\\ \Phi_{\text{REF}} &= u_1\,(\alpha\,R_{\text{PS}} + \beta\,R_{\text{SS}})\\ &\quad \exp[\,i\,\omega\,(\,y\,\sin\varphi_1 - z\,\cos\varphi_1 - u_1\,t\,)\,/\,u_1\,],\end{aligned} \tag{3}$$

moving back in medium 1, and transmitted waves

$$\begin{aligned}\Psi_{\text{TRA}} &= v_2\,(\alpha\,T_{\text{PP}} + \beta\,T_{\text{SP}})\\ &\quad \exp[\,i\,\omega\,(\,y\,\sin\psi_2 + z\,\cos\psi_2 - v_2\,t\,)\,/\,v_2\,]\\ \Phi_{\text{TRA}} &= u_2\,(\alpha\,T_{\text{PS}} + \beta\,T_{\text{SS}})\\ &\quad \exp[\,i\,\omega\,(\,y\,\sin\varphi_2 + z\,\cos\varphi_2 - u_2\,t\,)\,/\,u_2\,],\end{aligned} \tag{4}$$

moving forward in medium 2, where $(v_2\,,\,\psi_2)$ and $(u_2\,,\,\varphi_2)$ are respectively the velocity and transmitted angle of the P and S wave. The first subindex in the reflection and transmission coefficients indicates the nature of the incoming wave, P or S. The second subindex instead represents the type of the reflected and transmitted wave. The minus sign in the phase of the reflected potentials indicate the propagation in the direction of the negative z axis. The reflection and transmission angles are given by the Snell law:

$$\frac{\sin\psi_1}{v_1} = \frac{\sin\varphi_1}{u_1} = \frac{\sin\psi_2}{v_2} = \frac{\sin\varphi_2}{u_2}. \tag{5}$$

In Fig. 1, we show a schematic representation of incident, reflected and transmitted acoustic waves for granite/water and water/granite interfaces.

Due to the fact that the velocities are known and the angles are determined by the Snell law, the only quantities to be calculated are the reflection and transmission coefficients. These coefficients are obtained by imposing the continuity of displacement and stress across the interface. In terms of wave potentials, this means the continuity of the following functions:

$$\begin{aligned}&(1)\ \Psi_y - \Phi_z,\ \ (2)\ \Psi_z + \Phi_y,\ \ (3)\ \mu\,(2\,\Psi_{yz} + \Phi_{yy} - \Phi_{zz}),\\ &(4)\ \lambda\,(\Psi_{yy} + \Psi_{zz}) + 2\,\mu\,(\Psi_{zz} + \Phi_{yz}),\end{aligned} \tag{6}$$

where $\mu = \rho\,u^2$ and $\lambda = \rho\,(v^2 - 2\,u^2)$, with ρ the medium density and $u(v)$ the velocity of the S (P) wave. After simple algebraic manipulations, we can rewrite the equations coming from the continuity

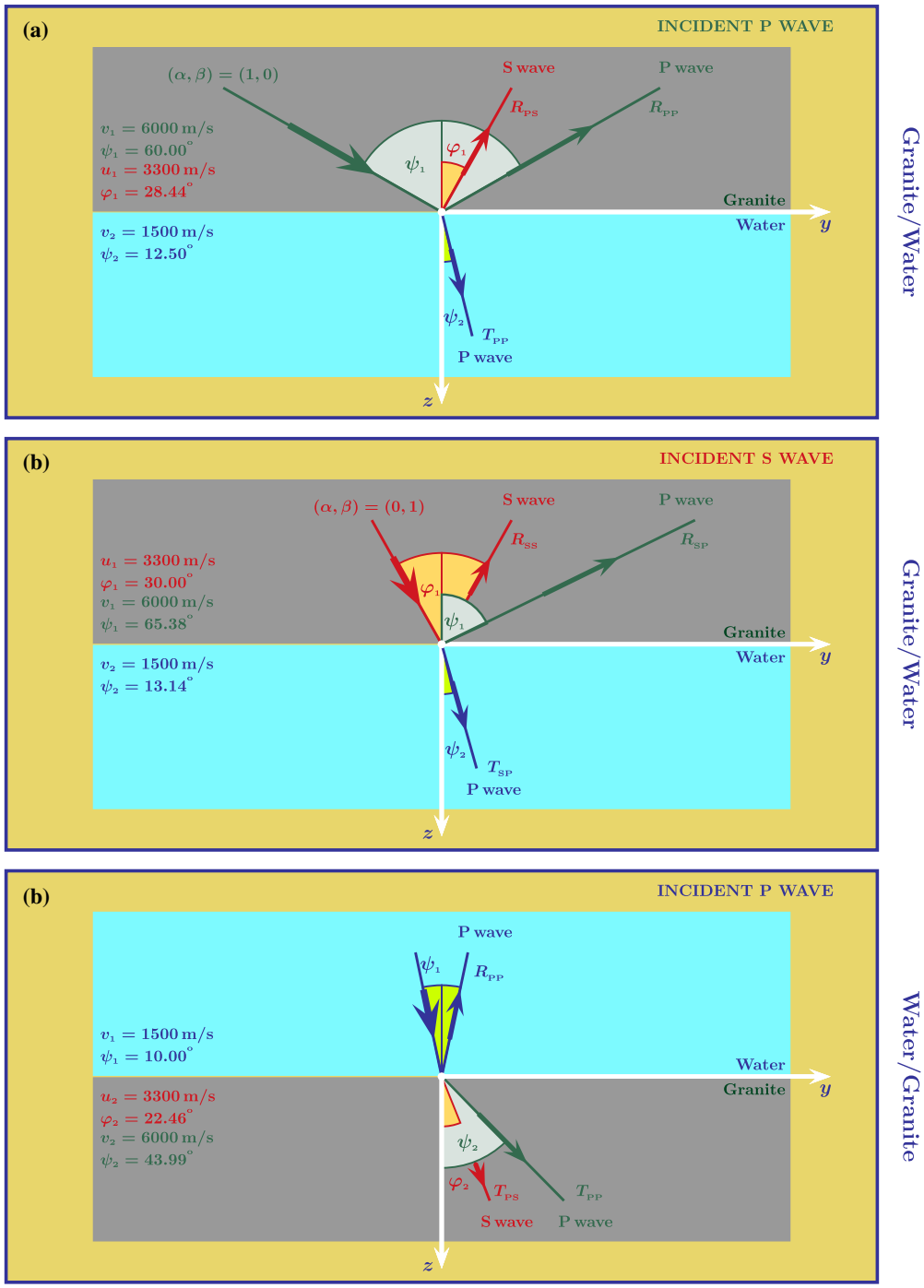

Schematic representation of incident, reflected and transmitted acoustic waves

Figure 1

Reflection and transmission acoustic waves for granite/water and eater/granite interfaces. In **a**, the incident P wave forms an angle of $\pi/3$ with the z axis. P and S waves are reflected in granite and P waves transmitted in the water. In **b**, the incident wave is an S wave and the incidence angle $\pi/6$. In **c**, the incident P wave forms an angle of $\pi/18$ with the z axis. P and S waves are transmitted in granite and P waves reflected in the water. The incidence angles was chosen to avoid evanescent waves

of displacement and stress in the following compact matrix form:

$$\mathcal{M}A = B, \tag{7}$$

where

$$\mathcal{M} = \begin{pmatrix} -\sin\psi_1 & -\cos\varphi_1 & \sin\psi_2 & -\cos\varphi_2 \\ \cos\psi_1 & -\sin\varphi_1 & \cos\psi_2 & \sin\varphi_2 \\ \rho_1 u_1^2 v_2 \sin 2\psi_1 & \rho_1 u_1 v_1 v_2 \cos 2\varphi_1 & \rho_2 u_2^2 v_1 \sin 2\psi_2 & -\rho_2 u_2 v_2 v_1 \cos 2\varphi_2 \\ -\rho_1 v_1 \cos 2\varphi_1 & \rho_1 u_1 \sin 2\varphi_1 & \rho_2 v_2 \cos 2\varphi_2 & \rho_2 u_2 \sin 2\varphi_2 \end{pmatrix}$$

and

$$A = \begin{pmatrix} \alpha R_{PP} + \beta R_{SP} \\ \alpha R_{PS} + \beta R_{SS} \\ \alpha T_{PP} + \beta T_{SP} \\ \alpha T_{PS} + \beta T_{SS} \end{pmatrix},$$

$$B = \begin{bmatrix} \alpha \sin\psi_1 - \beta \cos\varphi_1 \\ \alpha \cos\psi_1 + \beta \sin\varphi_1 \\ \rho_1 u_1 v_2 (\alpha u_1 \sin 2\psi_1 - \beta v_1 \cos 2\varphi_1) \\ \rho_1 (\alpha v_1 \cos 2\varphi_1 + \beta u_1 \sin 2\varphi_1) \end{bmatrix}.$$

The energy flux partitioning at the interface can be expressed in terms of the reflection and transmission coefficients appearing in Eq. (7) as follows:

$$\begin{aligned} E_{REF(P)} &= \alpha |R_{PP}|^2 + \beta \frac{v_1 \cos\psi_1}{u_1 \cos\varphi_1} |R_{SP}|^2, \\ E_{REF(S)} &= \alpha \frac{u_1 \cos\varphi_1}{v_1 \cos\psi_1} |R_{PS}|^2 + \beta |R_{SS}|^2, \\ E_{TRA(P)} &= \alpha \frac{\rho_2 v_2 \cos\psi_2}{\rho_1 v_1 \cos\psi_1} |T_{PP}|^2 + \beta \frac{\rho_2 v_2 \cos\psi_2}{\rho_1 u_1 \cos\varphi_1} |T_{SP}|^2, \\ E_{TRA(S)} &= \alpha \frac{\rho_2 u_2 \cos\varphi_2}{\rho_1 v_1 \cos\psi_1} |T_{PS}|^2 + \beta \frac{\rho_2 u_2 \cos\varphi_2}{\rho_1 u_1 \cos\varphi_1} |T_{SS}|^2. \end{aligned} \tag{8}$$

The Knott energy coefficients, given in Eq. (8), satisfy the energy conservation:

$$E_{REF(P)} + E_{REF(S)} + E_{TRA(P)} + E_{TRA(S)} = \alpha + \beta. \tag{9}$$

In the following Sections, we discuss the solid/liquid and liquid/solid scenarios and, once obtained the explicit solutions for the reflection and transmission coefficients, we give, for each case in which a critical region appears, the Goos–Hänchen phase, responsible for the lateral displacement of the reflected waves, and then discuss its properties. The graphical presentation of the results will be done using the media, velocities and densities listed in Table 1.

3. Solid–Liquid Interface: Incident S Waves

In the solid/liquid scenario, we can only have transmitted P waves ($u_2 = \varphi_2 = 0$). For the case of incident S wave ($\alpha = 0$ and $\beta = 1$), the Knott energy coefficients become

$$\begin{aligned} &\{E_{REF(P)}, E_{REF(S)}, E_{TRA(P)}, E_{TRA(S)}\} \\ &= \left\{ \frac{v_1 \cos\psi_1}{u_1 \cos\varphi_1} |R_{SP}|^2, |R_{SS}|^2, \frac{\rho_2 v_2 \cos\psi_2}{\rho_1 u_1 \cos\varphi_1} |T_{SP}|^2, 0 \right\} \end{aligned}$$

and the reflection and transmission coefficients are obtained by solving the reduced Zoeppritz matrix equation:

$$\begin{pmatrix} -\sin\psi_1 & -\cos\varphi_1 & \sin\psi_2 & -1 \\ \cos\psi_1 & -\sin\varphi_1 & \cos\psi_2 & 0 \\ u_1 \sin 2\psi_1 & v_1 \cos 2\varphi_1 & 0 & 0 \\ -\rho_1 v_1 \cos 2\varphi_1 & \rho_1 u_1 \sin 2\varphi_1 & \rho_2 v_2 & 0 \end{pmatrix} \begin{pmatrix} R_{SP} \\ R_{SS} \\ T_{SP} \\ T_{SS} \end{pmatrix} = \begin{pmatrix} -\cos\varphi_1 \\ \sin\varphi_1 \\ -v_1 \cos 2\psi_1 \\ \rho_1 u_1 \sin 2\varphi_1 \end{pmatrix}. \tag{10}$$

Table 1

In this table, we list the media, their densities, and the S and P wave velocities used to show graphical representations of the results obtained from our analysis

Medium	S wave velocity (m/s)	P wave velocity (m/s)	Density (g/cm^3)
Water	0	1500	1.0
Vegetal soil	300	700	2.4
Wet sand	600	2000	2.1
Granite	3300	6000	2.7

For an S wave incident upon a solid/liquid interface, we have four possible regions for the incidence angle φ_1: the region without critical angles:

$$0 < \varphi_1^{[a]} < \min\left[\arcsin\frac{u_1}{v_1}, \arcsin\frac{u_1}{v_2}\right], \qquad (11)$$

the region with evanescent transmitted P waves (and travelling reflected P and S waves):

$$\arcsin\frac{u_1}{v_2} < \varphi_1^{[b]} < \arcsin\frac{u_1}{v_1}, \qquad (12)$$

the region with evanescent reflected P waves (and travelling transmitted P and reflected S waves):

$$\arcsin\frac{u_1}{v_1} < \varphi_1^{[c]} < \arcsin\frac{u_1}{v_2}\ , \qquad (13)$$

and finally the region with evanescent reflected and transmitted P waves (and travelling reflected S waves):

$$\max\left[\arcsin\frac{u_1}{v_1}, \arcsin\frac{u_1}{v_2}\right] < \varphi_1^{[d]} < \frac{\pi}{2}. \qquad (14)$$

The critical angles for an incident S wave in the solid/liquid examples used in this paper are given in Table 2.

Table 2

Critical angles for S waves incident on vegetal soil/water, wet sand/water, and granite/water interfaces

Solid/liquid interface	Arcsin (u_1/v_1)	Arcsin (u_1/v_1)
Vegetal soil/water	25.38°	11.54°
Wet sand/water	17.46°	23.58°
Granite/water	33.37°	N/A

3.1. Incidence Rregion Before the Critical Angles

In this incidence region, $\cos\psi_1$ and $\cos\psi_2$ are both reals and we have two (P and S waves) reflected waves and a transmitted P wave. The Knott coefficients are given by

$$\begin{aligned}
E_{\mathrm{REF(P)}}^{[\mathrm{SoLiS}]} &= \frac{v_1\cos\psi_1}{u_1\cos\varphi_1}\left[\frac{2\,\rho_1 u_1 v_1 \sin 2\varphi_1 \cos 2\varphi_1 \cos\psi_2}{\rho_2 v_2 v_1 \cos\psi_1 + \rho_1\cos\psi_2\,(\,u_1^2\sin 2\psi_1 \sin 2\varphi_1 + v_1^2\cos^2 2\varphi_1\,)}\right]^2,\\
E_{\mathrm{REF(S)}}^{[\mathrm{SoLiS}]} &= \left[\frac{\rho_2 v_2 v_1\cos\psi_1 + \rho_1\cos\psi_2\,(\,-u_1^2\sin 2\psi_1\sin 2\varphi_1 + v_1^2\cos^2 2\varphi_1\,)}{\rho_2 v_2 v_1\cos\psi_1 + \rho_1\cos\psi_2\,(\,u_1^2\sin 2\psi_1\sin 2\varphi_1 + v_1^2\cos^2 2\varphi_1\,)}\right]^2, \qquad (15)\\
E_{\mathrm{TRA(P)}}^{[\mathrm{SoLiS}]} &= \frac{\rho_2 v_2\cos\psi_2}{\rho_1 u_1\cos\varphi_1}\left[\frac{2\,\rho_1 u_1 v_1\cos\psi_1\sin 2\varphi_1}{\rho_2 v_2 v_1\cos\psi_1 + \rho_1\cos\psi_2\,(\,u_1^2\sin 2\psi_1\sin 2\varphi_1 + v_1^2\cos^2 2\varphi_1\,)}\right]^2,
\end{aligned}$$

and satisfy the energy conservation equation:

$$E_{\mathrm{REF(P)}}^{[\mathrm{SoLiS}]} + E_{\mathrm{REF(S)}}^{[\mathrm{SoLiS}]} + E_{\mathrm{TRA(P)}}^{[\mathrm{SoLiS}]} = 1.$$

The upper limit of the incidence angles which guarantees real reflection and transmission coefficients and consequently 3 travelling waves with velocities u_1 (for S wave reflected in the first medium), v_1 (for P wave reflected in the first medium), v_2 (for P wave transmitted in the second medium), is then given by 11.54° for vegetal soil/water, 17.46° for wet sand/water, and 33.37° for granite/water, see Fig. 2.

3.2. Incidence Region with Evanescent Transmitted P Waves

This is the zone of the incidence region for which $u_1/v_2 < \sin\varphi_1 < u_1/v_1$. In this case,

$$\begin{aligned}
\cos\psi_2 &= \sqrt{1-\left(\frac{v_2}{u_1}\sin\varphi_1\right)^2}\\
&= i\sqrt{\left(\frac{v_2}{u_1}\sin\varphi_1\right)^2 - 1} = i\,|\cos\psi_2|,
\end{aligned}$$

the Knott coefficients become

$$
\begin{aligned}
lclE_{\mathrm{REF(P)}}^{[\mathrm{SoLiS}]} &= \frac{v_1 \cos\psi_1}{u_1 \cos\varphi_1} \left| \frac{2\, i\, \rho_1 u_1 v_1 \sin 2\varphi_1 \cos 2\varphi_1 |\cos\psi_2|}{\rho_2 v_2 v_1 \cos\psi_1 + i\, \rho_1 |\cos\psi_2| \,(u_1^2 \sin 2\psi_1 \sin 2\varphi_1 + v_1^2 \cos^2 2\varphi_1)} \right|^2, \\
E_{\mathrm{REF(S)}}^{[\mathrm{SoLiS}]} &= \left| \frac{\rho_2 v_2 v_1 \cos\psi_1 + i\, \rho_1 |\cos\psi_2| \,(-u_1^2 \sin 2\psi_1 \sin 2\varphi_1 + v_1^2 \cos^2 2\varphi_1)}{\rho_2 v_2 v_1 \cos\psi_1 + i\, \rho_1 |\cos\psi_2| \,(u_1^2 \sin 2\psi_1 \sin 2\varphi_1 + v_1^2 \cos^2 2\varphi_1)} \right|^2,
\end{aligned}
\tag{16}
$$

and satisfy the energy conservation

$$
E_{\mathrm{REF(P)}}^{[\mathrm{SoLiS}]} + E_{\mathrm{REF(S)}}^{[\mathrm{SoLiS}]} = 1.
$$

This scenario is for example reproduced in the presence of the vegetal soil/water interface for incidence angles between in 11.54° and 25.38°, as illustrated in Fig. 2a, b.

In this incidence region, both the P and S reflected waves gain an additional GH phase. For the P waves, the ZGH phase is

$$
\alpha_{\mathrm{GH}}^{[\mathrm{SoLiS}]} = -\arctan\left[\frac{\rho_1 |\cos\psi_2| \,(u_1^2 \sin 2\psi_1 \sin 2\varphi_1 + v_1^2 \cos^2 2\varphi_1)}{\rho_2 v_2 v_1 \cos\psi_1} \right] + \frac{\pi}{2},
\tag{17}
$$

and, for the S waves

$$
\begin{aligned}
rcl\beta_{\mathrm{GH}}^{[\mathrm{SoLiS}]} &= \arctan\left[\frac{\rho_1 |\cos\psi_2| \,(-u_1^2 \sin 2\psi_1 \sin 2\varphi_1 + v_1^2 \cos^2 2\varphi_1)}{\rho_2 v_2 v_1 \cos\psi_1} \right] \\
&\quad - \arctan\left[\frac{\rho_1 |\cos\psi_2| \,(u_1^2 \sin 2\psi_1 \sin 2\varphi_1 + v_1^2 \cos^2 2\varphi_1)}{\rho_2 v_2 v_1 \cos\psi_1} \right].
\end{aligned}
\tag{18}
$$

The energy conservation is now guaranteed by:

$$
E_{\mathrm{REF(S)}}^{[\mathrm{SoLiS}]} + E_{\mathrm{TRA(P)}}^{[\mathrm{SoLiS}]} = 1.
$$

This is for example the case of the wet sand/water interface for incidence angles in between 17.46° and 23.58°, see Fig. 2c, d, and of the granite/water interface for incidence angles greater than 33.37°, see Fig. 2e, f.

3.3. *Incidence Region with Evanescent Reflected P Waves*

For incidence angles in this region $(u_1/v_1 < \sin\varphi_1 < u_1/v_2)$ $\cos\psi_1 = i\,|\cos\psi_1|$ and the Knott coefficients are given by:

In this incidence region, for the S reflected we have the following ZGH phase:

$$
\begin{aligned}
E_{\mathrm{REF(S)}}^{[\mathrm{SoLiS}]} &= \left| \frac{i\, \rho_2 v_2 v_1 |\cos\psi_1| + \rho_1 \cos\psi_2 \,(-i\, u_1^2 |\sin 2\psi_1| \sin 2\varphi_1 + v_1^2 \cos^2 2\varphi_1)}{i\, \rho_2 v_2 v_1 |\cos\psi_1| + \rho_1 \cos\psi_2 \,(i\, u_1^2 |\sin 2\psi_1| \sin 2\varphi_1 + v_1^2 \cos^2 2\varphi_1)} \right|^2, \\
E_{\mathrm{TRA(P)}}^{[\mathrm{SoLiS}]} &= \frac{\rho_2 v_2 \cos\psi_2}{\rho_1 u_1 \cos\varphi_1} \left| \frac{2\, i\, \rho_1 u_1 v_1 |\cos\psi_1| \sin 2\varphi_1}{i\, \rho_2 v_2 v_1 |\cos\psi_1| + \rho_1 \cos\psi_2 \,(i\, u_1^2 |\sin 2\psi_1| \sin 2\varphi_1 + v_1^2 \cos^2 2\varphi_1)} \right|^2.
\end{aligned}
\tag{19}
$$

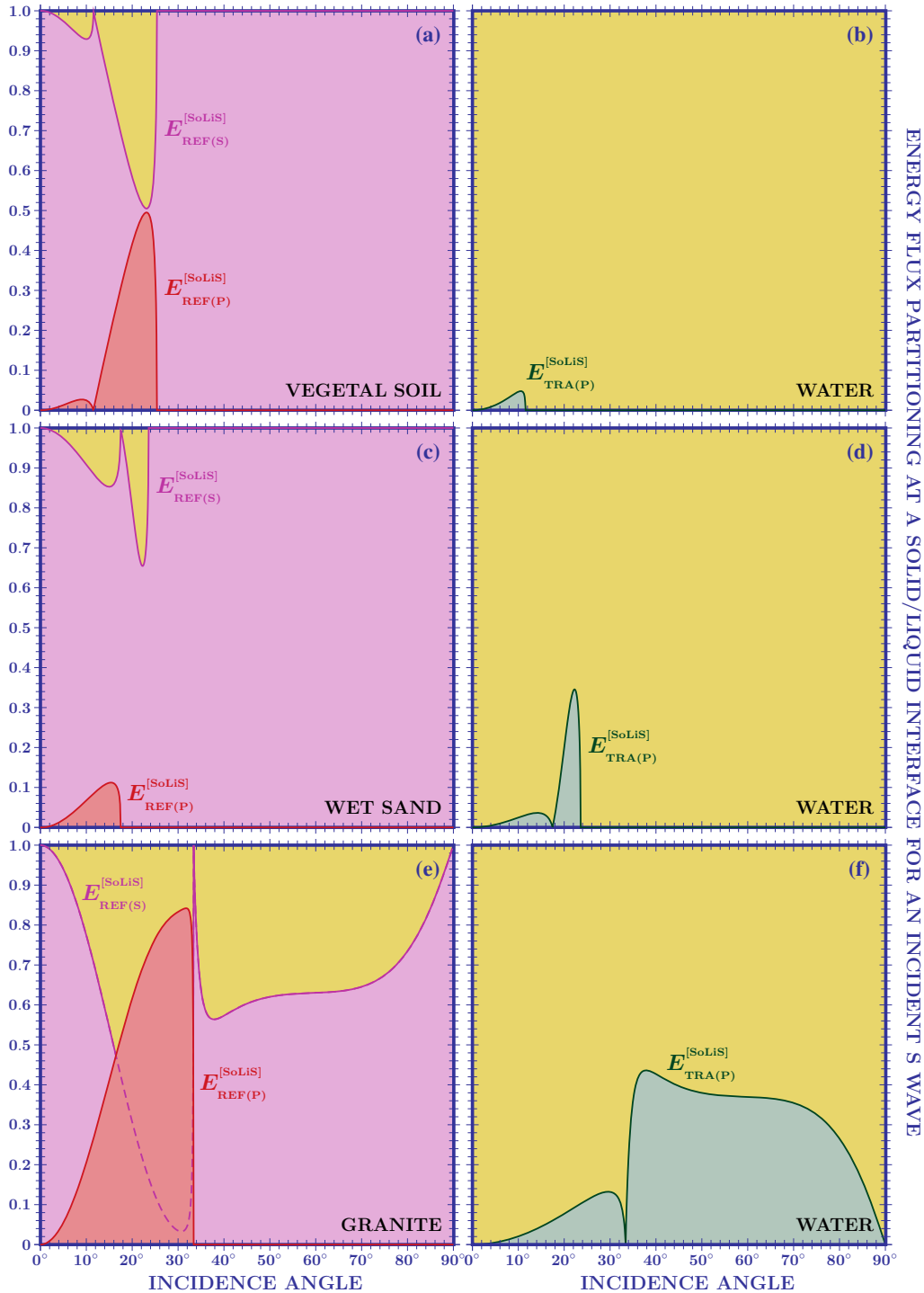

Figure 2
Energy flux partitioning at solid/liquid interfaces for an incident S wave. Three travelling waves are present for incidence lesser than the first critical angle, i.e., 11.54° for vegetal soil/water (**a**, **b**), 17.46° for wet sand/water (**c**, **d**), and 33.37° for granite/water (**e**, **f**). Total reflection induced by a complex coefficient occurs for S waves for incidence greater than the second critical angle, i.e., 25.38° for vegetal soil/water (**a**, **b**) and 23.58° for wet sand/water

$$rcly_{\mathrm{GH}}^{[\mathrm{SoLiS}]} = \arctan\left[\frac{\rho_2 v_2 v_1 |\cos\psi_1| - \rho_1 u_1^2 \cos\psi_2 |\sin 2\psi_1| \sin 2\varphi_1}{\rho_1 v_1^2 \cos\psi_2 \cos^2 2\varphi_1}\right] - \arctan\left[\frac{\rho_2 v_2 v_1 |\cos\psi_1| + \rho_1 u_1^2 \cos\psi_2 |\sin 2\psi_1| \sin 2\varphi_1}{\rho_1 v_1^2 \cos\psi_2 \cos^2 2\varphi_1}\right]. \tag{20}$$

3.4. Incidence Region with Evanescent Reflected and Transmitted P Waves

In this incidence region both $\cos\psi_1$ and $\cos\psi_2$ are imaginary and the Knott coefficient becomes

$$E_{\mathrm{REF(S)}}^{[\mathrm{SoLiS}]} = \left| \frac{i\,\rho_2 v_2 v_1 |\cos\psi_1| + i\,\rho_1 |\cos\psi_2|\,(-i\,u_1^2 |\sin 2\psi_1| \sin 2\varphi_1 + v_1^2 \cos^2 2\varphi_1)}{i\,\rho_2 v_2 v_1 |\cos\psi_1| + i\,\rho_1 |\cos\psi_2|\,(i\,u_1^2 |\sin 2\psi_1| \sin 2\varphi_1 + v_1^2 \cos^2 2\varphi_1)} \right|^2 = 1. \tag{21}$$

This is the scenario illustrated in the plots of Fig. 2 for vegetal soil/water (a, b) and wet sand/water (c, d) for incidence angles respectively greater than 25.38° and 23.58°.

The reflection coefficient for the S wave is given by $\exp\{i\,\delta_{\mathrm{GH}}^{[\mathrm{SoLiS}]}\}$ with

$$\delta_{\mathrm{GH}}^{[\mathrm{SoLiS}]} = -2\arctan\left[\frac{\rho_1 u_1^2 |\cos\psi_2 \sin 2\psi_1| \sin 2\varphi_1}{\rho_2 v_2 v_1 |\cos\psi_1| + \rho_1 v_1^2 |\cos\psi_2| \cos^2 2\varphi_1}\right]. \tag{22}$$

4. Solid–Liquid Interface: Incident P Waves

In the case of incident P waves ($\alpha = 1$ and $\beta = 0$) the Knott coefficients become

$$\{E_{\mathrm{REF(P)}}, E_{\mathrm{REF(S)}}, E_{\mathrm{TRA(P)}}, E_{\mathrm{TRA(S)}}\} = \left\{ |R_{\mathrm{PP}}|^2, \frac{u_1 \cos\varphi_1}{v_1 \cos\psi_1} |R_{\mathrm{PS}}|^2, \frac{\rho_2 v_2 \cos\psi_2}{\rho_1 v_1 \cos\psi_1} |T_{\mathrm{PP}}|^2, 0 \right\}$$

and the Zoeppritz matrix equation (7) reduces to

$$\begin{pmatrix} -\sin\psi_1 & -\cos\varphi_1 & \sin\psi_2 & -1 \\ \cos\psi_1 & -\sin\varphi_1 & \cos\psi_2 & 0 \\ u_1 \sin 2\psi_1 & v_1 \cos 2\varphi_1 & 0 & 0 \\ -\rho_1 v_1 \cos 2\varphi_1 & \rho_1 u_1 \sin 2\varphi_1 & \rho_2 v_2 & 0 \end{pmatrix} \begin{pmatrix} R_{\mathrm{PP}} \\ R_{\mathrm{PS}} \\ T_{\mathrm{PP}} \\ T_{\mathrm{PS}} \end{pmatrix} = \begin{pmatrix} \sin\psi_1 \\ \cos\psi_1 \\ u_1 \sin 2\psi_1 \\ \rho_1 v_1 \cos 2\varphi_1 \end{pmatrix}. \tag{23}$$

For incident P waves upon a solid/liquid interface, we only have two incidence regions:

$$0 < \psi_1^{[\mathrm{a}]} < \arcsin\frac{v_1}{v_2} < \psi_1^{[\mathrm{b}]} < \frac{\pi}{2}. \tag{24}$$

Indeed, due to the fact that $v_1 > u_1$, the angle of the reflected S wave will always be real. In the first region also the angle of the transmitted P wave is real and consequently the reflection and transmission coefficients are both real and no lateral displacement occurs. In the second region, $\cos\psi_2 = i\,|\cos\psi_2|$, and additional phases are found in the amplitudes of the reflected P and S waves.

The critical angles for an incident P wave in the solid/liquid examples used in this paper are given in Table 3.

4.1. Incidence Region Before the Critical Angle

In this incidence region the Knott coefficients are given in terms of real reflections and transmission coefficients,

$$
\begin{aligned}
E_{\mathrm{REF(P)}}^{[\mathrm{SoLiP}]} &= \left[\frac{\rho_2 v_2 v_1 \cos\psi_1 + \rho_1 \cos\psi_2 \,(\, u_1^2 \sin 2\psi_1 \sin 2\varphi_1 - v_1^2 \cos^2 2\varphi_1 \,)}{\rho_2 v_2 v_1 \cos\psi_1 + \rho_1 \cos\psi_2 \,(\, u_1^2 \sin 2\psi_1 \sin 2\varphi_1 + v_1^2 \cos^2 2\varphi_1 \,)}\right]^2 \\
E_{\mathrm{REF(S)}}^{[\mathrm{SoLiP}]} &= \frac{u_1 \cos\varphi_1}{v_1 \cos\psi_1}\left[\frac{2\,\rho_1 u_1 v_1 \sin 2\psi_1 \cos 2\varphi_1 \cos\psi_2}{\rho_2 v_2 v_1 \cos\psi_1 + \rho_1 \cos\psi_2 \,(\, u_1^2 \sin 2\psi_1 \sin 2\varphi_1 + v_1^2 \cos^2 2\varphi_1 \,)}\right]^2, \\
E_{\mathrm{TRA(P)}}^{[\mathrm{SoLiP}]} &= \frac{\rho_2 v_2 \cos\psi_2}{\rho_1 v_1 \cos\psi_1}\left[\frac{2\,\rho_1 v_1^2 \cos\psi_1 \cos 2\varphi_1}{\rho_2 v_2 v_1 \cos\psi_1 + \rho_1 \cos\psi_2 \,(\, u_1^2 \sin 2\psi_1 \sin 2\varphi_1 + v_1^2 \cos^2 2\varphi_1 \,)}\right]^2,
\end{aligned}
\tag{25}
$$

Table 3

Critical angles for P waves incident on vegetal soil/water, wet sand/water, and granite/water interfaces

Solid/liquid interface	Arcsin (v_1/v_2)
Vegetal soil/water	27.82°
Wet sand/water	N/A
Granite/water	N/A

and the energy conservation guaranteed by

$$
E_{\mathrm{REF(P)}}^{[\mathrm{SoLiP}]} + E_{\mathrm{REF(S)}}^{[\mathrm{SoLiP}]} + E_{\mathrm{TRA(P)}}^{[\mathrm{SoLiP}]} = 1.
$$

This scenario is illustrated in the plots of Fig. 3c–f for wet sand/water and granite/water for all incidence angles. For the case of vegetal soil/water, we find three travelling waves for incidence angles before the critical angle 27.82°, see Fig. 3a, b.

4.2. Incidence Region After the Critical Angle

For incidence angles greater than the critical one, we have evanescent transmitted P waves and the Knott coefficients become

$$
\begin{aligned}
E_{\mathrm{REF(P)}}^{[\mathrm{SoLiP}]} &= \left|\frac{\rho_2 v_2 v_1 \cos\psi_1 + i\,\rho_1 |\cos\psi_2| \,(\, u_1^2 \sin 2\psi_1 \sin 2\varphi_1 - v_1^2 \cos^2 2\varphi_1 \,)}{\rho_2 v_2 v_1 \cos\psi_1 + i\,\rho_1 |\cos\psi_2| \,(\, u_1^2 \sin 2\psi_{|1} \sin 2\varphi_1 + v_1^2 \cos^2 2\varphi_{|1} \,)}\right|^2, \\
E_{\mathrm{REF(S)}}^{[\mathrm{SoLiP}]} &= \frac{u_1 \cos\varphi_1}{v_1 \cos\psi_1}\left|\frac{2\,i\,\rho_1 u_1 v_1 \sin 2\psi_1 \cos 2\varphi_1 |\cos\psi_2|}{\rho_2 v_2 v_1 \cos\psi_1 + i\,\rho_1 |\cos\psi_2| \,(\, u_1^2 \sin 2\psi_1 \sin 2\varphi_1 + v_1^2 \cos^2 2\varphi_1 \,)}\right|^2,
\end{aligned}
\tag{26}
$$

and satisfy

$$
E_{\mathrm{REF(P)}}^{[\mathrm{SoLiP}]} + E_{\mathrm{REF(S)}}^{[\mathrm{SoLiP}]} = 1.
$$

In this case, the P and S reflected wave gain respectively the following phases:

$$
\begin{aligned}
\alpha_{\mathrm{GH}}^{[\mathrm{SoLiP}]} &= \arctan\left[\frac{\rho_1 |\cos\psi_2| \,(\, u_1^2 \sin 2\psi_1 \sin 2\varphi_1 - v_1^2 \cos^2 2\varphi_1 \,)}{\rho_2 v_2 v_1 \cos\psi_1}\right] \\
&\quad - \arctan\left[\frac{\rho_1 |\cos\psi_2| \,(\, u_1^2 \sin 2\psi_1 \sin 2\varphi_1 + v_1^2 \cos^2 2\varphi_1 \,)}{\rho_2 v_2 v_1 \cos\psi_1}\right],
\end{aligned}
\tag{27}
$$

and

$$
\beta_{\mathrm{GH}}^{[\mathrm{SoLiP}]} = \arctan\left[\frac{\rho_1 |\cos\psi_2| \,(\, u_1^2 \sin 2\psi_1 \sin 2\varphi_1 + v_1^2 \cos^2 2\varphi_1 \,)}{\rho_2 v_2 v_1 \cos\psi_1}\right] + \frac{\pi}{2}.
\tag{28}
$$

5. Liquid–Solid Interface

In this scenario, we can only have incident and reflected P waves. Consequently, we have to set $\alpha = 1$, $\beta = 0$, and $u_1 = \varphi_1 = 0$ in the Zoeppritz matrix equation (7). The Knott energy coefficients reduce to

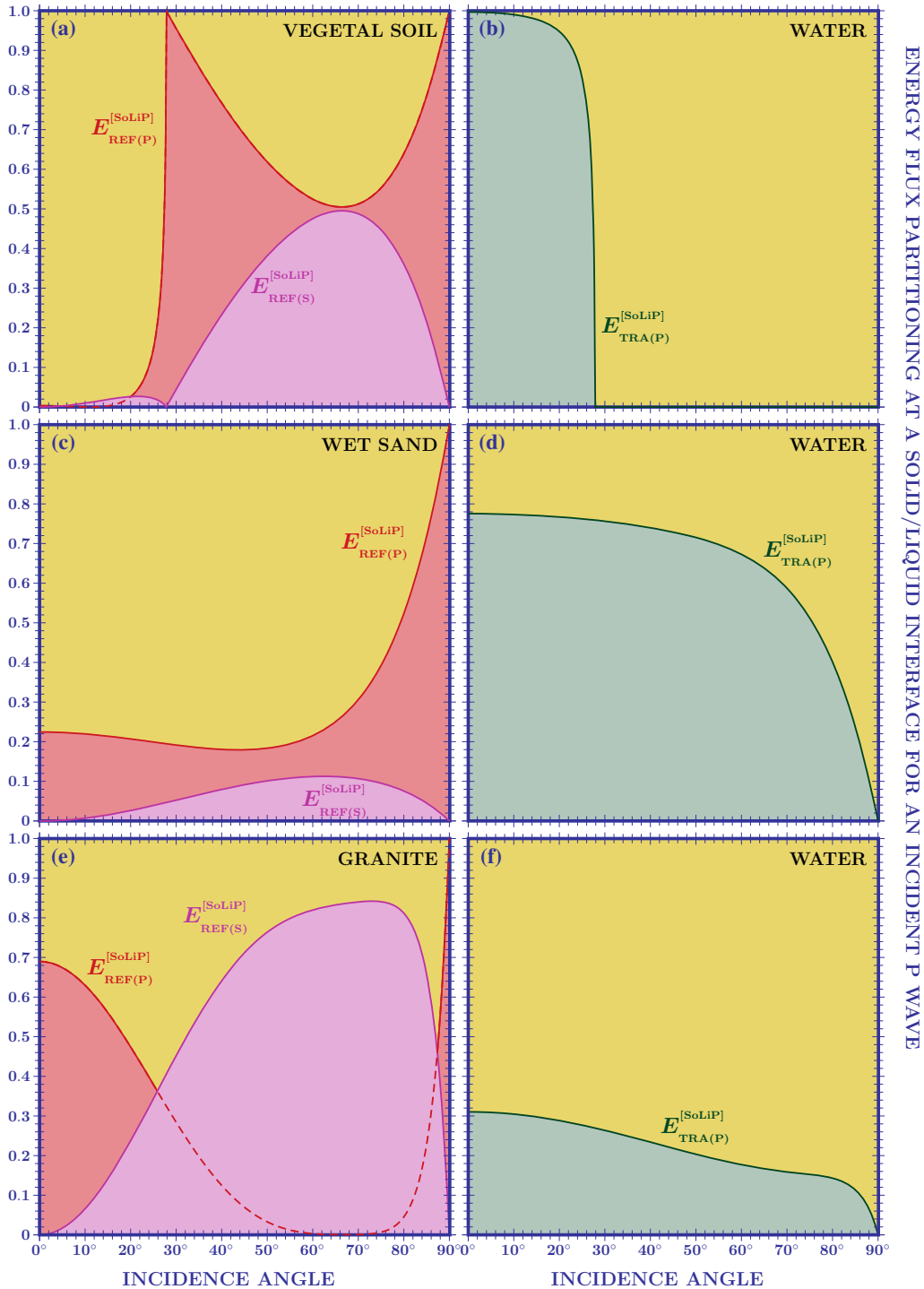

Figure 3

Energy flux partitioning at solid/liquid interfaces for an incident P wave. For wet sand/water (**c**, **d**) and granite/water (**e**, **f**), three travelling waves are found for all incidence angles. For vegetal soil/water (**a**, **b**) this occurs for incidence before the critical angle 27.82°. Total reflection induced by a complex coefficient is not present in these scenarios

$$\{E_{\mathrm{REF(P)}}, E_{\mathrm{REF(S)}}, E_{\mathrm{TRA(P)}}, E_{\mathrm{TRA(S)}}\} = \left\{ |R_{\mathrm{PP}}|^2, 0, \frac{\rho_2 v_2 \cos\psi_2}{\rho_1 v_1 \cos\psi_1} |T_{\mathrm{PP}}|^2, \frac{\rho_2 u_2 \cos\varphi_2}{\rho_1 v_1 \cos\psi_1} |T_{\mathrm{PS}}|^2 \right\}$$

and the reflection and transmission coefficients will be determined by solving the Zoeppritz matrix equation:

$$\begin{pmatrix} -\sin\psi_1 & -1 & \sin\psi_2 & -\cos\varphi_2 \\ \cos\psi_1 & 0 & \cos\psi_2 & \sin\varphi_2 \\ 0 & 0 & u_2 \sin 2\psi_2 & -v_2 \cos 2\varphi_2 \\ -\rho_1 v_1 & 0 & \rho_2 v_2 \cos 2\varphi_2 & \rho_2 u_2 \sin 2\varphi_2 \end{pmatrix} \begin{pmatrix} R_{\mathrm{PP}} \\ R_{\mathrm{PS}} \\ T_{\mathrm{PP}} \\ T_{\mathrm{PS}} \end{pmatrix} = \begin{pmatrix} \sin\psi_1 \\ \cos\psi_1 \\ 0 \\ \rho_1 v_1 \end{pmatrix}. \tag{29}$$

For a liquid/solid interface, we find three distinct incidence subregions:

$$0 < \psi_1^{[\mathrm{I}]} < \arcsin\frac{v_1}{v_2} < \psi_1^{[II]} < \arcsin\frac{v_1}{u_2} < \psi_1^{[\mathrm{III}]} < \frac{\pi}{2}. \tag{30}$$

The critical angles for an incident P wave in the liquid/solid examples used in this paper are given in Table 4.

5.1. First incidence region

In the first incidence region $\cos\psi_2$ and $\cos\varphi_2$, are both real and consequently we have a travelling (back) reflected P wave and two travelling (forward) transmitted P and S waves with Knott energy coefficients given by

Table 4

Critical angles for P waves incident on water/vegetal soil, water/wet sand, and water/granite interfaces

Liquid/solid interface	Arcsin (v_1/v_2)	Arcsin (v_1/u_2)
Water/vegetal soil	N/A	N/A
Water/wet sand	48.59°	N/A
Water/granite	14.48°	27.04°

and satisfying

$$E_{\mathrm{REF(P)}}^{[\mathrm{LiSo}]} + E_{\mathrm{TRA(P)}}^{[\mathrm{LiSo}]} + E_{\mathrm{TRA(S)}}^{[\mathrm{LiSo}]} = 1.$$

This is for example the case of water/vegetal soil for all the incidence angles, see Fig. 4a, b. For water/wet sand and water/granite interfaces this scenario is respectively seen before the critical angles 48.59°, Fig. 4c, d, and 14.48°, see Fig. 4e, f.

5.2. Second Incidence Region

This is the incidence region for which only the transmitted P angle is imaginary, $\cos\psi_2 = i|\cos\psi_2|$. In this case, we have an evanescent transmitted P and a travelling transmitted S wave. the Knott coefficients are given by

$$\begin{aligned} E_{\mathrm{REF(P)}}^{[\mathrm{LiSo}]} &= \left[\frac{\rho_2 \cos\psi_1 (v_2^2 \cos^2 2\varphi_2 + u_2^2 \sin 2\psi_2 \sin 2\varphi_2) - \rho_1 v_1 v_2 \cos\psi_2}{\rho_2 \cos\psi_1 (v_2^2 \cos^2 2\varphi_2 + u_2^2 \sin 2\psi_2 \sin 2\varphi_2) + \rho_1 v1 v_2 \cos\psi_2} \right]^2 \\ E_{\mathrm{TRA(P)}}^{[\mathrm{LiSo}]} &= \frac{\rho_2 v_2 \cos\psi_2}{\rho_1 v_1 \cos\psi_1} \left[\frac{2\rho_1 v1 v_2 \cos\psi_1 \cos 2\varphi_2}{\rho_2 \cos\psi_1 (v_2^2 \cos^2 2\varphi_2 + u_2^2 \sin 2\psi_2 \sin 2\varphi_2) + \rho_1 v1 v_2 \cos\psi_2} \right]^2 \\ E_{\mathrm{TRA(S)}}^{[\mathrm{LiSo}]} &= \frac{\rho_2 u_2 \cos\varphi_2}{\rho_1 v1 \cos\psi_1} \left[\frac{2\rho_1 v_1 u_2 \cos\psi_1 \sin 2\psi_2}{\rho_2 \cos\psi_1 (v_2^2 \cos^2 2\varphi_2 + u_2^2 \sin 2\psi_2 \sin 2\varphi_2) + \rho_1 v1 v_2 \cos\psi_2} \right]^2 \end{aligned} \tag{31}$$

$$E_{\mathrm{REF(P)}}^{[\mathrm{LiSo}]} = \left| \frac{\rho_2 \cos\psi_1 (v_2^2 \cos^2 2\varphi_2 + i u_2^2 |\sin 2\psi_2| \sin 2\varphi_2) - i \rho_1 v_1 v_2 |\cos\psi_2|}{\rho_2 \cos\psi_1 (v_2^2 \cos^2 2\varphi_2 + i u_2^2 |\sin 2\psi_2| \sin 2\varphi_2) + i \rho_1 v1 v_2 |\cos\psi_2|} \right|^2,$$
$$E_{\mathrm{TRA(S)}}^{[\mathrm{LiSo}]} = \frac{\rho_2 u_2 \cos\varphi_2}{\rho_1 v_1 \cos\psi_1} \left| \frac{2 i \rho_1 v_1 u_2 \cos\psi_1 |\sin 2\psi_2|}{\rho_2 \cos\psi_1 (v_2^2 \cos^2 2\varphi_2 + i u_2^2 |\sin 2\psi_2| \sin 2\varphi_2) + i \rho_1 v1 v_2 |\cos\psi_2|} \right|^2, \tag{32}$$

and they guarantee the energy conservation

$$E_{\mathrm{REF(P)}}^{[\mathrm{LiSo}]} + E_{\mathrm{TRA(S)}}^{[\mathrm{LiSo}]} = 1.$$

The reflected P wave becomes complex and gains the following GH phase:

$$\alpha_{\mathrm{GH}}^{[\mathrm{LiSo}]} = \arctan\left(\frac{\rho_2 \cos\psi_1 u_2^2 |\sin 2\psi_2| \sin 2\varphi_2 - \rho_1 v_1 v_2 |\cos\psi_2|}{\rho_2 \cos\psi_1 v_2^2 \cos^2 2\varphi_2} \right) - \arctan\left(\frac{\rho_2 \cos\psi_1 u_2^2 |\sin 2\psi_2| \sin 2\varphi_2 + \rho_1 v_1 v_2 |\cos\psi_2|}{\rho_2 \cos\psi_1 v_2^2 \cos^2 2\varphi_2} \right). \tag{33}$$

This is for example the case illustrated in Fig. 4c, d after the critical angle 48.59° (water/wet sand) and in Fig. 4e, f between in 14.48° and 27.04° (water/granite).

5.3. Third Incidence Region

In the last incidence subregion both the transmitted P and S waves are evanescent and the Knott coefficient for the reflected P wave becomes

$$E_{\mathrm{REF(P)}}^{[\mathrm{LiSo}]} = \left| \frac{\rho_2 \cos\psi_1 (v_2^2 \cos^2 2\varphi_2 - u_2^2 |\sin 2\psi_2 \sin 2\varphi_2|) - i \rho_1 v_1 v_2 |\cos\psi_2|}{\rho_2 \cos\psi_1 (v_2^2 \cos^2 2\varphi_2 - u_2^2 |\sin 2\psi_2 \sin 2\varphi_2|) + i \rho_1 v_1 v_2 |\cos\psi_2|} \right|^2 = 1. \tag{34}$$

The reflection coefficient for the reflected P wave is then given by $\exp\{ i \beta_{\mathrm{GH}}^{[\mathrm{LiSo}]} \}$ with

$$\beta_{\mathrm{GH}}^{[\mathrm{LiSo}]} = -2 \arctan\left[\frac{\rho_1 v_1 v_2 |\cos\psi_2|}{\rho_2 \cos\psi_1 (v_2^2 \cos^2 2\varphi_2 - u_2^2 |\sin 2\psi_2 \sin 2\varphi_2|)} \right]. \tag{35}$$

This scenario is for example seen in Fig. 4e, f for incidence angles greater than 27.04° (water/granite interface).

6. Lateral Displacements

In Artmann (1948), used the method of stationary phase and, analyzing the additional phase of the Fresnel coefficients describing the total reflection of optical waves, theoretically explained the lateral displacement for transverse electric (TE) waves observed, one year before, by Goos and Hänchen. He also predicted a different displacement for transverse magnetic (TM) waves, experimentally confirmed in Goos and Hänchen (1949).

In this section, we briefly introduce the Artmann analytical tool to find the lateral shift of optical waves and then apply it to find the lateral displacements of reflected seismic P and S waves. In doing it, let us introduce a real angle distribution, $g(\theta, \theta_0)$, centered in θ_0, the angle of incidence of an optical beam upon a dielectric/air interface. This angular distribution allows to determine the behavior of the incident and reflected wave packets through the integrals

incident wave: $\int \mathrm{d}\theta\, g(\theta, \theta_0) \exp[ik(\sin\theta y + \cos\theta z)]$

and

reflected wave: $\int \mathrm{d}\theta\, g(\theta, \theta_0)\, R(\theta)$ $\exp[\, i k\, (\, \sin\theta\, y\, -\, \cos\theta\, z\,)\,]$,

where $R(\theta)$ is the Fresnel coefficient for the reflected wave obtained by solving the Maxwell equations and imposing the field continuity conditions. The

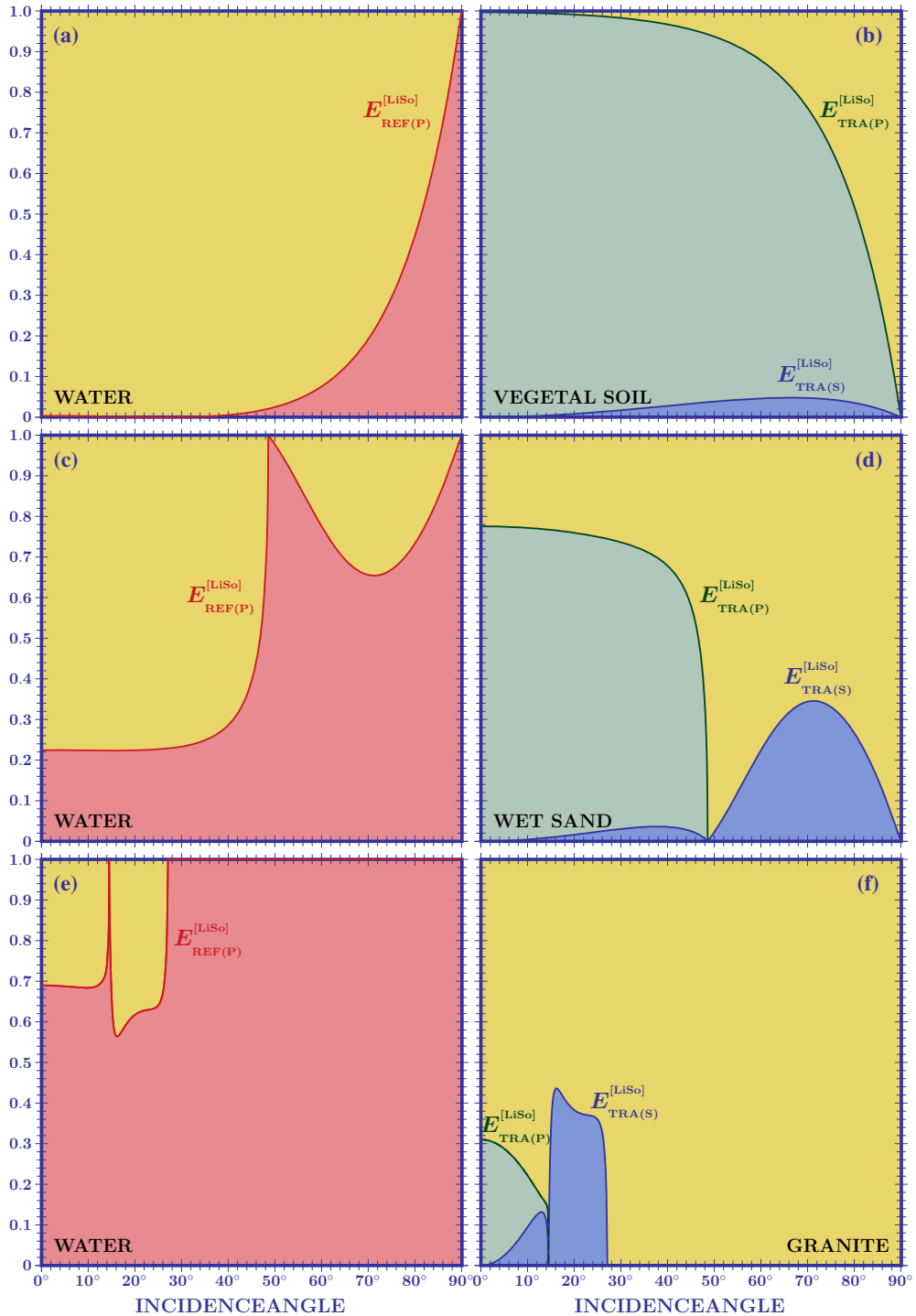

Figure 4
Energy flux partitioning at liquid/solid interfaces for an incident P wave. Three travelling waves are found for incidence lesser than the first critical angle, i.e., 48.59° for wet sand/water (**c**, **d**) and 14.48° for granite/water (**e**, **f**), and for all the incidence angles for vegetal soil/water (**a**, **b**). Total reflection induced by a complex reflection coefficient occurs for incidence angles greater than the second critical angle, i.e., 27.04° for granite/water (**e**, **f**)

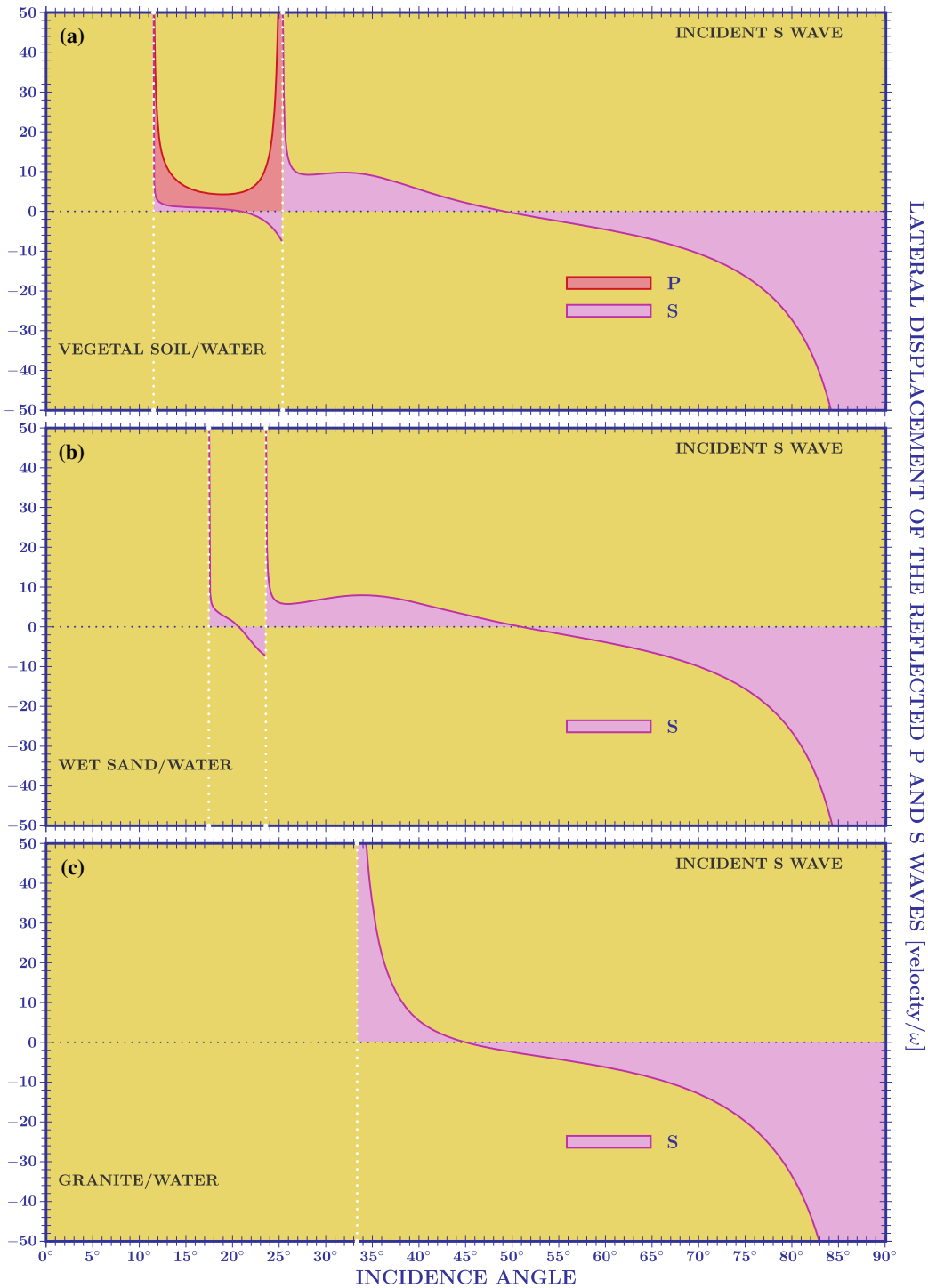

Figure 5

Lateral displacement in the solid/liquid scenarios for the reflected P and S waves in the case of an incidence S wave. In the regime of total internal reflection, after the second critical angle 25.38° for vegetal soil/water (**a**, **b**) and after 23.58° for wet sand/water (**c**, **d**), a new maximum appears. This behavior is not present in optics. The divergences at critical angles are typical of the plane wave approach and they can be removed using the wave packet formalism

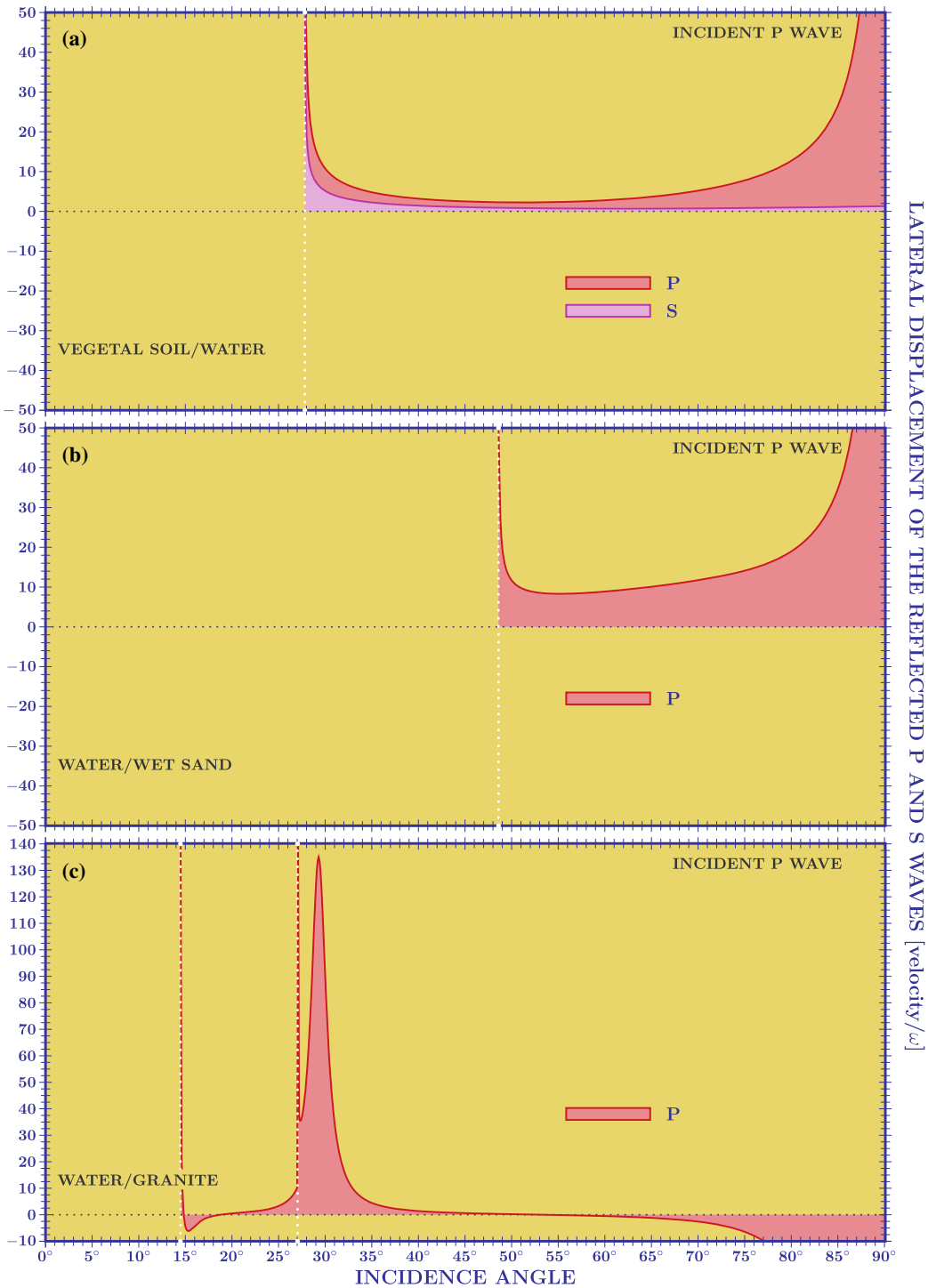

Figure 6
Lateral displacement in the solid/liquid (**a**) and liquid/solid (**b**, **c**) scenarios for the reflected P and S waves in the case of an incidence P wave. In the water/granite case (**c**), for total internal reflection, i.e., incidence angles greater than 27.04°, after the second critical angle we observe the presence of an incidence angle which maximizes the lateral shift

stationary phase method idea is used to estimate the beam propagation without solving the integrals. This can be done by observing that asymptotically, when the phase is large enough to generate rapid oscillations, the integrand contributions cancel out, except at stationary points, i.e., the points where the phase derivative is null. For the incident wave this happens for

$$[\partial_\theta(k\sin\theta y + k\cos\theta z)]_0 = 0 \quad \Rightarrow \quad y_{\text{inc}} = \tan\theta_0 z.$$

When the reflection coefficient is complex, $|R(\theta)|\exp[i\Phi_{\text{GM}}(\theta)]$, the spatial phase of the reflected wave gains an additional phase. Using the method of stationary phase, we find

$$\{\partial_\theta[k\sin\theta y - k\cos\theta z + \Phi_{\text{GH}}(\theta)]\}_0 = 0$$
$$\Rightarrow \quad y_{\text{ref}} = -\tan\theta_0 z - \Phi'_{\text{GH}}(\theta_0)/k\cos\theta_0.$$

Observing that $k = 2\pi/\lambda$, the lateral displacement of the reflected optical beam is proportional to λ. Due to the fact that the Fresnel coefficients are different from TE and TM, the lateral shift also depends on the light polarization.

In the case of seismic waves incident on a solid/liquid interface, we have, in general, two reflected waves and consequently we have to distinguish between two lateral displacements, the Compressional or Primary GH (PGH) shift:

$$y_{\text{ref}}^{[\text{P}]} = -\tan\psi_1 z - \frac{v_1}{\omega\cos\psi_1}\frac{\partial\Phi_{\text{GH}}}{\partial\psi_1} \tag{36}$$

and the Shear or Secondary GH (SGH) shift:

$$y_{\text{ref}}^{[\text{S}]} = -\tan\varphi_1 z - \frac{u_1}{\omega\cos\varphi_1}\frac{\partial\Phi_{\text{GH}}}{\partial\varphi_1}. \tag{37}$$

Lateral displacements for both the P and S reflected waves are found for incoming S waves in the following incidence region

$$\arcsin\frac{u_1}{v_2} < \varphi_1 < \arcsin\frac{u_1}{v_1}$$

and for incoming P waves for

$$\arcsin\frac{v_1}{v_2} < \psi_1 < \frac{\pi}{2}.$$

This happens when the liquid P wave velocity is greater than the velocity of the P (and consequently S) wave propagating in the solid. For the examples examined in this paper, this only occurs for the vegetal soil/water scenario. We find lateral displacements for both the P and S reflected waves, for incident S waves between the angle 11.54° and 25.38°, see Fig. 5a, and for incident P waves after the angle 27.82°, see Fig. 6a.

In optics, we always have total reflection for an incidence angle greater than the critical one. In the seismic solid/liquid case, total reflection is only reached for incident S waves when

$$\max\left[\arcsin\frac{u_1}{v_1}, \arcsin\frac{u_1}{v_2}\right] < \varphi_1 < \frac{\pi}{2}.$$

The lateral displacement for totally reflected S waves is shown in Fig. 5 for vegetal soil/water after 25.38° (a) and for wet sand/water after 23.58° (b).

For the liquid/solid scenario, the incidence angle condition which guarantees total reflection for P waves is

$$\arcsin\frac{v_1}{u_2} < \psi_1 < \arcsin\frac{\pi}{2}.$$

This means that the propagation velocity of S waves in the solid has to be greater than the velocity of the P waves propagating in the liquid. This, for example, happens for the water/granite case when in incidence angle is greater than 27.04°, see Fig. 6c.

It is interesting to observe that we have total reflection when the following two condition are simultaneously satisfied: two critical angles appear and the incidence angle is in the third incidence region, i.e., in the region where the incidence angle is greater than the second critical angle, see Figs. 5a, b and 6c. In these cases, with respect to the optical case, a completely new phenomenon occurs. The presence of a maximum just after the second critical angle. In particular, this is clearly evident for the liquid/solid case where the GH phase is

$$\beta_{\text{GH}}^{[\text{LiSo}]} = -2\arctan\left[\frac{\rho_1 v_1 v_2|\cos\psi_2|}{\rho_2\cos\psi_1(v_2^2\cos^2 2\varphi_2 - u_2^2|\sin 2\psi_2\sin 2\varphi_2|)}\right].$$

The study of the derivative of this phase is shown in Fig. 7 for different values of ρ_2/ρ_1, u_2/v_1, and v_2/v_1. In Fig. 7a, we see that, for equal ratios of the solid/liquid propagation velocities, changing density ratio the maximum of the lateral displacement changes proportionally to the density ratio but practically at

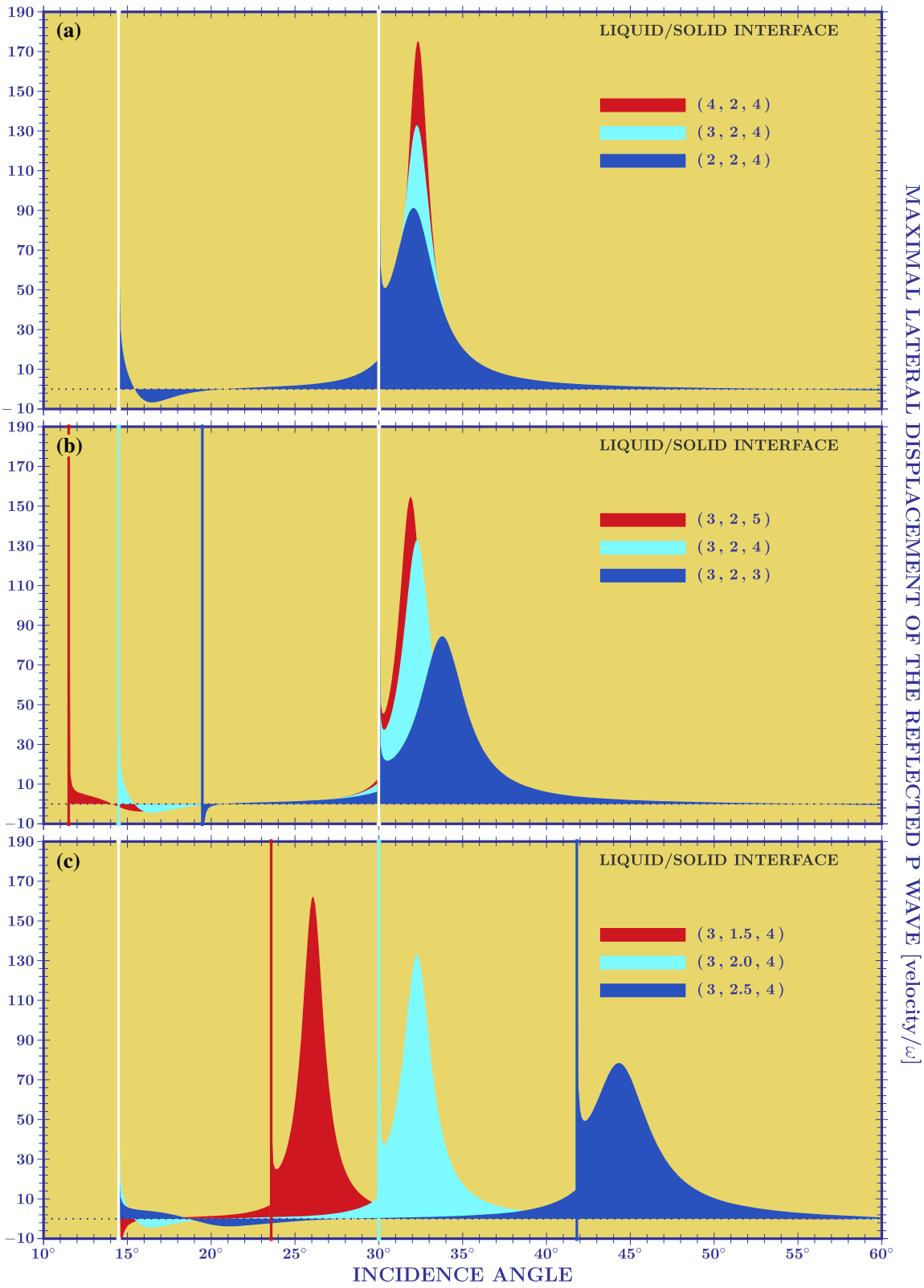
(a)
LIQUID/SOLID INTERFACE
(4, 2, 4)
(3, 2, 4)
(2, 2, 4)
(b)
LIQUID/SOLID INTERFACE
(3, 2, 5)
(3, 2, 4)
(3, 2, 3)
(c)
LIQUID/SOLID INTERFACE
(3, 1.5, 4)
(3, 2.0, 4)
(3, 2.5, 4)
190
170
150
130
110
90
70
50
30
10
−10
10° 15° 20° 25° 30° 35° 40° 45° 50° 55° 60°
INCIDENCE ANGLE
MAXIMAL LATERAL DISPLACEMENT OF THE REFLECTED P WAVE [velocity/ω]

◀Figure 7
Lateral displacement for the liquid/solid scenario for different density and velocity ratios. In **a**, the velocity ratios $u_2 = 2\,v_1$ and $v_2 = 4v_1$ are fixed and the density ratio is varied $\rho_2 = (4,\,3\,,2)\,\rho_1$. The effect of the velocity ratio variation is analyzed in (**b**) where $\rho_2 = 3\,\rho_1$, $u_2 = 2\,v_1$, $v_2 = (5,\,4\,,3)\,v_1$ and in (**c**) where $\rho_2 = 3\,\rho_1$, $v_2 = 4\,v_1$, $u_2 = (1.5,\,2.0\,,2.5)\,v_1$

the same incidence angle. The liquid/solid phase is of the form $\arctan[\mathrm{num}/\rho\mathrm{den}]$, and consequently the lateral displacement given by $\rho(\mathrm{num}'\mathrm{den} - \mathrm{num}\mathrm{den}')/(\mathrm{num}^2 + \rho^2\,\mathrm{den}^2)$. The plots of Fig. 7a then suggests that the incidence angle, for which a maximum shift is found, is obtained by solving

$$v_2^2 \cos^2 2\varphi_2 = u_2^2 |\sin 2\psi_2 \sin 2\varphi_2|. \tag{38}$$

Observing that

$$\sin\varphi_2 = \frac{u_2}{v_1}\sin\psi_1, \qquad \cos\varphi_2 = i\sqrt{\left(\frac{u_2}{v_1}\sin\psi_1\right)^2 - 1},$$
$$\sin\psi_2 = \frac{v_2}{v_1}\sin\psi_1, \qquad \cos\psi_2 = i\sqrt{\left(\frac{v_2}{v_1}\sin\psi_1\right)^2 - 1},$$

the previous equation can be rewritten as follows:

$$v_2^2\left[1 - 2\left(\frac{u_2}{v_1}\sin\psi_1\right)^2\right]^2 = 4\,\frac{u_2^3 v_2}{v_1^2}\sin^2\psi_1 \sqrt{\left(\frac{u_2}{v_1}\sin\psi_1\right)^2 - 1}\sqrt{\left(\frac{v_2}{v_1}\sin\psi_1\right)^2 - 1}. \tag{39}$$

After simple algebraic manipulations, we find a polynomial equation in the variable $x = \sin^2\psi_1$:

$$16\,u^6\,(v^2 - u^2)\,x^3 + 8\,u^4\,(2\,u^2 - 3\,v^2)\,x^2 + 8\,u^2\,v^2\,x - v^2 = 0, \tag{40}$$

where $u = u_2/v_1$ and $v = v_2/v_1$. This polynomial equation allows to calculate, in the liquid/solid scenario, the incidence angle at which the GH lateral displacement is maximized. For a water/granite interface, $u = 33/15$ and $v = 4$, Eq. (40) gives a real solution at $x \approx 0.2416$. Consequently, the incidence angle which maximize the GH lateral shift is found at

$$\psi_1^{[\max]} = \arcsin\sqrt{0.2416} = 29.44^\circ,$$

see Fig. 6c.

The divergence at the critical angle and the discontinuity between the region before and after the critical incidence have recently been discussed and solved, in optics, using the wave packet formalism (Araújo et al. 2014a, b; Aráujo et al. 2017). It was also proven that the plane wave analysis remains correct outside the critical region:

$$\left[\theta_{\mathrm{cri}} - \frac{\lambda}{\mathrm{w}_0},\, \theta_{\mathrm{cri}} + \frac{\lambda}{\mathrm{w}_0}\right],$$

where the phase in the integrand can be approximated using the stationary phase method and the integral analytically solved (Aráujo et al. 2016). This clearly also occurs for seismic waves. This means that the plane wave analysis presented in this paper reproduces the correct results for incidence angle outside the critical regions.

Of particular interest are the cases in which total reflection for a single wave occurs. In such cases, we find a maximum after the second critical angle and this effect is amplified in the liquid/solid scenario. As observed before, the plane wave analysis is valid outside the critical region. The maximum obtained in the plane wave analysis is thus valid also for wave packet with a beam waist w_0 if critical angle, maximal angle, velocities, frequency, and beam waist satisfy

$$\psi_1^{[\max]} > \arcsin\frac{v_1}{u_2} + \frac{v_1}{\omega\,\mathrm{w}_0}.$$

For a water/granite interface and incident waves with a frequency 10 KHz, this implies the following constraint on the beam waist:

$$\mathrm{w}_0 > \frac{0.15\ \mathrm{m}}{29.44 - 27.04}\,\frac{180}{\pi} \approx 3.5\,\mathrm{m}.$$

7. *Conclusions*

The study of the GH shift has been a continuous source of excitement in the optics community. Since its first experimental evidence in Goos and Hänchen (1947), the central interests were the theoretical understanding of the phenomenon and the possibility to find analytical expressions for predicting the lateral displacements. The first analytical formula, based on the stationary phase method, was given by Artmann

(1948). He observed that when the light is totally reflected the reflection coefficient becomes complex and the additional phase is responsible for the shift.

Even being true that the plane wave approach contains divergences that can only be removed using the wave packet formalism (Aráujo et al. 2016, 2017), it is important to recall that, outside the critical region, the plane wave approach gives results in full agreement with the ones obtained using wave packets. In this spirit, using plane waves and the stationary phase method, we presented a detailed analysis of lateral displacements of the reflected P and S waves in the solid/liquid and liquid/solid scenarios, confident that, as it is done in optics, the divergences at critical angles can later be removed by treating the problem within the wave packet formalism.

The Goos–Hänchen effect is a phenomenon of classical optics in which a light beam reflecting off a surface is spatially shifted as a consequence of its brief penetration through the surface before bouncing back. The same phenomenon occurs for acoustic waves where, due to the matrix structure of the Zoeppritz equations, in general, two critical angles are found. In seismic data, contrary to what happens in optics, a total reflection can occur also for real reflection coefficients. In this case, no lateral shift is observed in the reflected wave. This is for example the case of reflected S waves in the vegetal soil/water, wet sand/water and granite/water scenarios for incidence at 11.54°, 17.46°, and 33.37°, see Fig. 2a, c, e, and of reflected P waves in the vegetal soil/water, water/wet sand, and water/granite scenarios for incidence at 27.82°, 48.59°, and 14.48°, see Figs. 3a and 4c, e.

The analysis presented in this paper shows positive and negative lateral displacements for the reflected S and P waves and the presence of a local maximum shift just after the second critical angle, see for example the case of reflected S waves in the vegetal soil/water and wet sand/water scenarios for incidence greater than 25.38° and 23.58°, see Fig. 5a, b and the case of reflected P waves in water/granite scenario for incidence greater that 27.04°, see Fig. 6c. In this last case, the lateral displacement is huge, for example for incident P waves of a frequency of 10 KHz, we find a lateral displacement of approximatively 20.25 m (135 × 0.15 m), see Fig. 6c. In seismic analysis, these maximal lateral displacements have to be included in the theoretical predictions to avoid discrepancies between experimental data and computational simulations.

The main goals of the study presented in this article are to offer a basic formal mathematical introduction to the GH effect in seismic data analysis, to solve the Zoeppritz equations, to explicitly give the complex phase of the reflection coefficients in the solid/liquid and liquid/solid scenarios from which the lateral displacement can be calculated using the stationary phase method, and finally to find the polynomial equation allowing the prediction of the incidence angle which maximizes the ZGH lateral displacement, see Eq. (40). In obtaining such an equation, the simulations presented in Fig. 7, where the density and velocity ratios were varied, played a fundamental role.

Usually the analogies between different physical systems help to gain an increased understanding of the phenomenon studied and sometimes open the door to new effects and challenges. The study of the ZGH effect for acoustic waves is an intriguing example of this. Clearly, there still exist several open questions such as a closed formula for the maximum lateral displacement, the shift analysis for critical incidence, and the breaking of symmetry near the critical region.

Deviations from geometrical optics are not restricted to lateral displacements. Indeed, the spatial GH shift has an angular analogous effect (White et al. 1977; Chan and Tamir 1985; Araújo et al. 2017). This effect has recently been observed in optical experiment for incidence in the resonant Brewster region (Merano et al. 2009), using a transverse electric wave to decouple the polarization from the propagation dynamics of the beam (Merano et al. 2010), and by the weak measurement technique (Jayaswal et al. 2014). The angular deviations of the beam axis with respect to the ray optics prediction appear in the incidence region of partial reflection in contrast with the lateral displacements which occur when the light is totally reflected. While the spatial GH shift is essentially due to the phase of the Fresnel reflection coefficient, the angular effect is mainly connected to the amplitude of the Fresnel reflection

coefficient. Consequently, it is the breaking of symmetry in the optical beam wave number distribution induced by the Fresnel reflection coefficient to cause the angular deviation (Araújo et al. 2017). Such a breaking of symmetry can also be seen for acoustic (scalar) waves when the reflection Zoeppritz coefficient rapidly changes, see Figs. 2, 3 and 4 and thus this effect is not restricted to the vector nature of light. Of particular interest, it could be, for example, to examine the Rayleigh waves influence on acoustic beams at liquid–solid interfaces (Bertoni and Tamir 1973; Declercq and Lamkanfi 2008) in view of the double peak reflected beam recently discussed in optics (Araújo et al. 2017).

Seismic negative lateral displacements simulate the negative GH shifts found in optics (Bonnet et al. 2001; Lai and Chan 2002; Chen et al. 2007) and should be addressed in terms of destructive interference between the incident and reflection waves.

These topics deserve further investigations within the wave packet formalism. The authors feeling is that this work only represents a first step in this direction and the hope is that the study presented in this paper could stimulate further investigations and forthcoming articles on this subject.

Acknowledgements

The authors sincerely thank Dr. Gabriel G. Maia for helpful mathematical discussions, numerical checking, and stimulating conversations during the preparation of the manuscript.

References

Aharonov, Y., Albert, D. Z., & Vaidman, L. (1988). How the result of a measurement of a component of the spin of a spin 1/2 particle can turn out to be 100. *Physical Review Letters*, *60*, 1351–1354.

Aiello, A. (2012). Goos–Hänchen and Imbert-Federov shifts: a novel perspective. *New Journal of Physics*, *14*, 013058.

Araújo, M. P., Carvalho, S. A., & De Leo, S. (2014). Maximal breaking of symmetry at critical angle and closed-form expression for angular deviations of the Snell law. *Physical Review A*, *90*, 033844.

Araújo, M., Carvalho, S. A., & De Leo, S. (2014). The asymmetric Goos–Hänchen effect. *Journal of Optics*, *160*, 15702–7.

Araújo, M. P., De Leo, S., & Maia, G. G. (2015). Axial dependence of optical weak measurements in the critical region. *Journal of Optics*, *17*, 035608–035610.

Aráujo, M. P., De Leo, S., & Maia, G. G. (2016). Closed-form expression for the Goos–Hänchen lateral displacement. *Physical Review A*, *930*, 23801–23810.

Aráujo, M. P., De Leo, S., & Maia, G. G. (2017). Oscillatory behavior of light in the composite Goos–Haenchen shift. *Physical Review A*, *95*, 053836–053839.

Araújo, M., De Leo, S., & Maia, G. (2017). Optimizing weak measurements to detect angular deviations. *Annalen der Physik (Berlin)*, *529*, 1600357.

Artmann, K. (1948). Berechnung der Seitenversetzung des totalreflektierten Strahles. *Annalen der Physik*, *437*, 87–102.

Ashcroft, W. (2011). *A petroleum geologist's guide to seismic reflection*. New Jersey: Wiley-Blackwell.

Bertoni, H. L., & Tamir, T. (1973). Unified theory of Rayleigh angle phenomena for ccoustic beams at liquid–solid interfaces. *Applied Physics*, *2*, 157–172.

Bliokh, K. Y., & Aiello, A. (2013). Goos-Hänchen and Imbert-Fedorov beam shifts: an overview. *Journal of Optics*, *15*, 014001–014016.

Bliokh, K. Y., & Aiello, A. (2013). Electronic analogy of the Goos Haenchen effect: a review. *Journal of Optics*, *15*, 033001–033012.

Bonnet, C., Chauvat, D., Emile, O., Bretenaker, F., & Le Floch, A. (2001). Measurement of positive and negative Goos Hänchen effects for metallic gratings near wood anomalies. *Optics Letters*, *26*, 666–668.

Chan, C. C., & Tamir, T. (1985). Angular shift of a Gaussian beam reflected near the Brewster angle. *Optics Letters*, *10*, 378–380.

Chen, L., Cao, Z., Ou, F., Li, H., Shen, Q., & Qiao, H. (2007). Observation of large positive and negative lateral shifts of a reflected beam from symmetrical metal-cladding waveguides. *Optics Letters*, *32*, 1432–1434.

Declercq, N. F., & Lamkanfi, E. (2008). Study by means of liquid side acoustic barrier of the influence of leaky Rayleigh waves on bounded beam reflection. *Applied Physics Letters*, *93*, 054103.

Duck, I. M., & Stevenson, P. M. (1989). The sense in which a weak measurement of a spin 1/2 particles spin component yields a value 100. *Physical Review D*, *40*, 2112–2117.

Goos, F., & Hänchen, H. (1947). Ein neuer und fundamentaler Versuch zur Totalreflexion. *Annalen der Physik*, *436*, 333–346.

Goos, F., & Hänchen, H. (1949). Neumessung des Strahlwersetzungseffektes bei totalreflexion. *Annalen der Physik*, *440*, 251–252.

Ignatovich, V. K. (2004). Neutron reflection from condensed matter, the Goos–Haenchen effect and coherence. *Physics Letters A*, *32*, 236–46.

Ikelle, L. T., & Amundsen, L. (2005). Introduction to petroleum seismology. *Society of Exploration Geophysicists*, *12*, 1–26. https://doi.org/10.1190/1.9781560801702.

Jayaswal, G., Mistura, G., & Merano, M. (2013). Weak measurement of the Goos-Hänchen shift. *Optics Letters*, *38*, 1232–1234.

Jayaswal, G., Mistura, G., & Merano, M. (2014). Observing angular deviations in light-beam reflection via weak measurements. *Optics Letters*, *39*, 6257–6260.

Lai, H. M., & Chan, S. W. (2002). Large and negative Goos Hänchen shift near the Brewster dip on reflection from weakly absorbing media. *Optics Letters*, *27*, 680–682.

Lerche, I. (1990). Reflection of wide-angle acoustic waves from a high velocity interface. *Pure and Applied Geophysics*, *134*, 109–115.

Liu, F. P., Gao, J., Li, R. Z., Wang, A. L., Chen, H. G., & Yang, C. C. (2008). The influence on normal moveout of totally reflected sv-wave by Goos-Hänchen effect at a free surface of stratum. *Chinese Journal of Geophysics*, *51*, 617–624.

Liu, F. P., Meng, X. J., Xiao, J. Q., Wang, A. L., & Yang, C. C. (2012). The Goos–Haenchen shift of wide-angle seismic reflection wave. *Science China Earth Sciences*, *55*, 852–857.

Merano, M., Aiello, A., van Exter, M. P., & Woerdman, J. P. (2009). Observing angular deviations in the specular reflection of a light beam. *Nature Photonics*, *3*, 337–340.

Merano, M., Hermosa, N., Aiello, A., & Woerdman, J. P. (2010). Demonstration of a quasi-scalar angular Goos Hänchen effect. *Optics Letters*, *35*, 3562–3564.

Ostrander, W. J. (1984). Plane-wave reflection coefficients for gas sands at nonnormal angles of incidence. *Geophysics*, *49*, 1637–48.

Santana, O., Carvalho, S., De Leo, S., & de Araújo, L. (2016). Weak measurement of the composite Goos–Hänchen shift in the critical region. *Optics Letters*, *41*, 3884–3887.

Upadhyay, S. K. (2004). *Seismic reflection processing*. Berlin: Springer.

Wang, Z. (2015). The influence of the Goos Haenchen effect on seismic data processing and AVO in attenuating media. *Journal of Applied Geophysics*, *122*, 122–133.

White, I. A., Snyder, A. W., & Pask, C. (1977). Directional change of beams undergoing partial reflection. *Journal of the Optical Society of America*, *67*, 703–705.

(Received November 21, 2017, revised January 14, 2018, accepted January 16, 2018, Published online February 2, 2018)